Particle segregation in inclined high-speed granular flows

Aurélien Neveu, Michele Larcher, Renaud Delannay, James T. Jenkins, Alexandre Valance

Particle segregation in inclined high-speed granular flows

Aurélien Neveu[1], Michele Larcher[2], Renaud Delannay[1], James T. Jenkins[3] and Alexandre Valance[1]

[1] IPR, Univ Rennes, CNRS UMR 6251, Campus Beaulieu, F-35042 Rennes, France
[2] Free University of Bozen-Bolzano, Faculty of Science and Technology, Bolzano, Italy
[3] School of Civil and Environmental Engineering, Cornell University, Ithaca, New York, USA

(Received January 14, 2022)

We report on the discovery, using numerical simulations, of a segregation pattern in high-speed granular flows, in which size segregation is primarily driven by two-dimensional granular temperature gradients, rather than by gravity. In contrast to slower flows on gentle slopes, in high speed flows on steep slopes, large particles no longer accumulate in the upper layers of the flow, but are trapped in the interior. The strong temperature gradients that develop between the interior of the flow and the surrounding dilute periphery appear to govern the segregation mechanism. Interestingly, these new segregated flows run at a much faster speed than similar mono-disperse flows. This opens up promising perspectives for transporting granular material with enhanced efficiency. Importantly, we show that the kinetic theory for dense, inclined flows of binary mixtures can provide a relevant theoretical framework to explain the segregation patterns observed in the numerical simulations.

1. Introduction

Granular mixture of particles that differ in size or density tend to demix into striking segregation patterns (e.g., radial segregation in rotating drums (Hill *et al.* 2004; Gray & Ancey 2011), granular fingering (Pouliquen *et al.* 1997), or self-induced Rayleigh-Taylor instability (D'Ortona & Thomas 2020)). Various factors influence the segregation patterns, including gravity, gradients of concentration and granular temperature, and secondary flows. Among these, segregation attributed purely to gravity has been studied the most (Savage & Lun 1988; Khakhar *et al.* 1997; Gray & Thornton 2005); however the role played by gradients in the granular temperature is beginning to be understood (Arnarson & Jenkins 2004; Larcher & Jenkins 2013, 2015); with spheres of two sizes made of the same material, the larger migrate towards regions of lower granular temperature, for spheres of the same size made of different materials, the more massive move downward under gravity. Slow and dense gravitational flows of poly-sized granular mixture have earned serious attention. In many of these flows, larger particles migrate at the surface of the flow while smaller ones percolate to the bottom. The dominant mechanisms driving this segregation process is commonly identified as kinetic sieving and squeeze expulsion (Savage & Lun 1988).

Recently, Brodu *et al.* (2015) highlighted the existence of highly inhomogeneous flows on steep slopes, named "supported flows" (Taberlet *et al.* 2007) and characterized by a dense core floating over a dilute and highly agitated layer of grains. We present here discrete numerical simulations that reveal a new segregation pattern emerging in high-speed granular flows, in which large particles are trapped within the flow in the dense core.

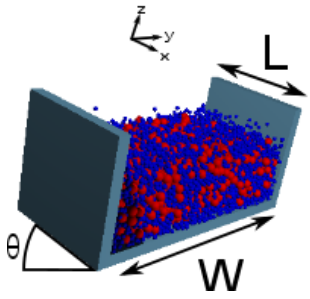

FIGURE 1. Scheme of the simulation cell of width W and length L. The flow is bounded by infinitely high (in z direction) flat walls in the transverse direction y, and periodic boundary conditions are applied in the stream direction x. The box is inclined by an angle θ.

This size segregation is driven by granular temperature gradients rather than gravity and can be described by the kinetic theory for binary mixtures. The granular temperature is a measure of the energy of the velocity fluctuations of the grains. Interestingly, this segregating behavior promotes the transport capability of the flow of binary mixtures, which can be one of the mechanisms involved in long run-out avalanches observed in nature. A flow enhancement due simply to the presence of spheres of two sizes is also predicted by kinetic theory (Larcher & Jenkins 2019) for particle-fluid flows.

2. Simulation methodology

To unravel the role of complex secondary flows on the segregation process of a granular mixture of spheres, numerical simulations using the Discrete Element Method (DEM) have been performed. The details of the method can be found in Brodu *et al.* (2013). We recall here briefly the main ingredients. The simulation cell is composed of smooth, flat and frictional bottom and parallel side walls (see Figure 1), in a similar way that is usually done experimentally (Louge & Keast 2001; Richard *et al.* 2008). The simulation cell width W is chosen to be $W = 40\,D$, with D a unit of length, and periodic boundary conditions are applied in the stream-wise direction with a periodic length $L = 20\,D$. The cell is tilted by an angle θ to produce flows. Particles are subject to gravity and interact through frictional visco-elastic contacts with other particles. These interactions employ a linear visco-elastic model with normal and tangential coefficients of restitution $e_n^{gg} = 0.972$ and $e_t^{gg} = 0.25$, respectively. The normal spring stiffness is chosen as $k_n^{gg} = 2\text{x}10^5 m^* g/D$, with m^* and g being mass and acceleration units, respectively; the tangential spring stiffness is computed from the relation provided by Brodu *et al.* (2013): $7k_t^{gg}(\pi^2 + [ln(e_n^{gg})]^2) = 2k_n^{gg}(\pi^2 + [ln(e_t^{gg})]^2)$. The tangential force is bounded according to a Coulomb friction model with friction coefficient μ^{gg}. The same set of parameters is used for particles/wall contacts: $e_n^{gw} = 0.8$, $e_t^{gw} = 0.35$, $k_n^{gw} = 2\text{x}10^5$, $\mu^{gw} = 0.593$. These parameter values are taken from Louge & Keast (2001) and correspond to glass beads and aluminum walls to match materials usually used in experiments.

A time step of $2\text{x}10^{-5}\sqrt{(D/g)}$ was chosen as a good compromise between numerical stability requirements and reasonable simulation duration. The total mass in the system is controlled by the mass holdup, which basically represents the height of the grain assembly when densely packed and is defined by $H = \sum_i m_i/(\rho^* LW)$, with $\rho^* = 6m^*/\pi D^3$, the reference material density, and m_i, the mass of the grain i. All the simulation outcomes have been obtained with a mass hold-up $H = 6D$. Binary mixtures have been used. The two grain species have the same material density ρ^*, but differ in size, with a mean radii r_S and r_L, respectively, for the small and large. The radii of each size are uniformly distributed by 8% around the mean value. The radius of the "mixture sphere" is defined

as the average of both radii, $r = (r_S + r_L)/2$. The grains have masses m_S and m_L, with $m = m_S + m_L$, number densities, n_S and n_L, with $n = n_S + n_L$, and mass densities, $\rho_S = m_S n_S$ and $\rho_L = m_L n_L$, with $\rho = \rho_S + \rho_L$. We define volume concentrations for the small and large grains, $c_S = 4\pi n_S r_S^3/3$ and $c_L = 4\pi n_L r_L^3/3$, and for the mixture $c = c_S + c_L$, and we denote the volume concentration fraction of the small particles in the mixture as $\Phi_S = c_S/c$, which is equivalent to the mass concentration fraction for grains made of same material. The granular temperature T of the mixture is defined as: $T = (n_S T_S + n_L T_L)/n$ where $T_i = (1/2)m_i < (\mathbf{v_i} - \mathbf{V}) .(\mathbf{v_i} - \mathbf{V}) >$ with $i = S, L$ ($\mathbf{v_i}$ is the particle velocity of species i and $\mathbf{V}$ is the barycentric velocity of the mixture).

Most of the simulation outcomes were obtained for binary mixtures with a radii ratio $r_L/r_S = 2$ and a mixture diameter $2r = 1.125D$ (i.e., $2r_S = 0.75D$ and $2r_S = 1.5D$) and various volume concentration fraction Φ_S of small particles ranging from 0 to 100%. For the comparison with the kinetic theory, we also employed mixtures with a smaller radii ratio $r_L/r_S = 1.35$ and a mixture diameter $2r = 1D$ (i.e., $2r_S = 0.85D$ and $2r_L = 1.15D$). The particles of the mixture were initially displayed on a regular lattice but randomly distributed between the small and large according to the prescribed volume concentration fraction. The assembly of particles is dropped at a small altitude from the bottom of cell with a finite but small stream-wise velocity $V_x = 5\sqrt{gD}$. After a transient which never exceeds $1000\sqrt{(D/g)}$ time units, for the set of parameters investigated so far, the flow reaches a steady state in which flow kinematic and segregation patterns remain stationary (i.e., relative variations are less than 1%). We explored a large range of inclination angles (from 19 to 50°) for various mass concentration fraction of the mixture and the flow always achieved a steady state. The coarse-grained fields (volume fraction, velocity and granular temperature) are computed following Serero *et al.* (2008) with a Lucy polynomial for the weighting function as proposed by Weinhart *et al.* (2012). The window size of the coarse-graining procedure is twice the mean particle diameter, i.e., $2(r_L + r_S)$. The field values are spatially averaged along the stream-wise direction and time averaged over 200 time units, once the flow reached its steady state.

3. Supported flows and segregation patterns

As a start, we describe briefly the main features of the flow regimes obtained for monodisperse particles with diameter $2r = 1D \pm 0.08D$. Packing fraction and longitudinal velocity maps of the flow cross-section for three different inclination angles are presented in Fig. 2. For a low inclination angle ($\theta = 19°$), a dense unidirectional flow is observed with grains arranged in horizontal layers. At an intermediate angle ($\theta = 25°$), the layering is broken and a denser region emerged within the flow accompanied with a pair of counter-rotating longitudinal rolls. One can note a slight concavity of the free surface with a trough in the center of the cell. At a higher inclination angle ($\theta = 35°$), a supported state develops. The latter is characterized by the presence of a very dense core surrounded by a dilute layer of highly agitated grains. This scenario that leads to the emergence of supported flows was already evidenced by Brodu *et al.* (2015) for wider channels ($W = 68D$) and is also observed with smaller gap widths Zhu *et al.* (2021). For $W = 40D$, the transition towards supported flows occurs at a critical inclination angle $\theta_c = 27°$.

We first investigated the segregation patterns obtained for a binary mixture with equal mass (i.e., equivalently, equal volume) of small and large particles ($\Phi_S = 0.5$) and with a size ratio equal to 2 (i.e., $2r_L = 1.5D$ and $2r_S = 0.75$). Figure 3 shows the relative local concentration of large particles c_L/c within the flow cross-section for three inclination angles (19°, 25° and 35°), together with streamlines to visualize the longitudinal rolls. For an inclination of 19°, the flow is unidirectional and uniformly sheared and a classical

(a)

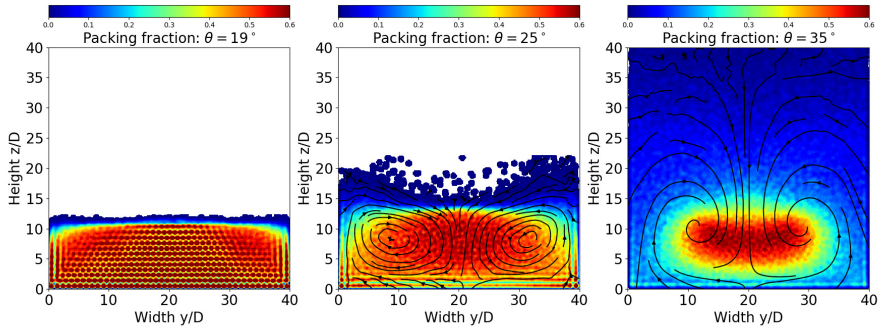

(b)

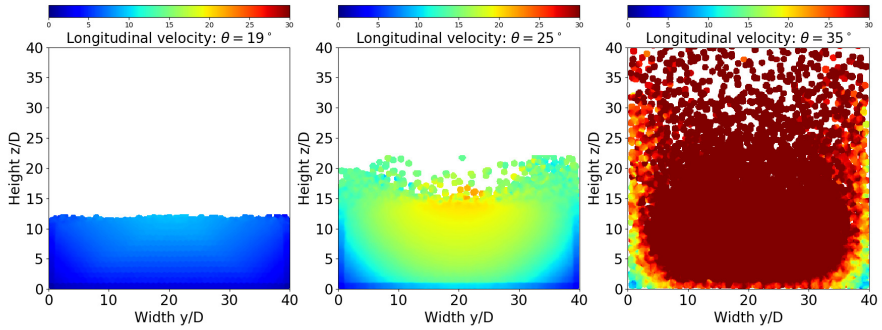

FIGURE 2. Monodisperse flows ($2r = 1D$) for $H = 6D$ and $W = 40D$: (a) Packing fraction maps together with transverse velocity (black lines) for a dense flow ($\theta = 19°$), an intermediate flow ($\theta = 25°$) and a supported flow ($\theta = 35°$), as already evidenced in (Brodu *et al.* 2015) for a wider channel. (b) Corresponding longitudinal velocities

reverse grading is observed, with large particles at the top of the flow, while small particles have percolated down to the bottom.

Upon increasing the inclination angle (i.e. $\theta \approx 25°$), a pair of longitudinal rolls develops within the flow. The convection tends to mix the granular systems, because large particles are incorporated in the bulk flow. A transverse segregation also clearly appears: there is a depletion of large particles between the two longitudinal rolls. At higher inclination (i.e., $\theta = 30°$), as in the monodisperse case, a supported flow regime emerges with a dense core "floating" over a highly agitated and dilute layer. Despite the formation of the dense core, convection rolls are still present. Surprisingly, the setting of this supported state leads to the emergence of a new segregation pattern in which the large particles no longer reside at the surface of the flow but are trapped within the dense, cooler core, as clearly evidenced for $\theta = 35°$. More precisely, two spots of high concentration of large grains are located at the center of the longitudinal rolls, surrounded by a mixed layer of large and small particles. Pure layers of small particles are present close to the bottom and lateral walls, and the upper part of the flows consists essentially of small particles. This segregated state is not a transient but a mature and steady state. An intermediate

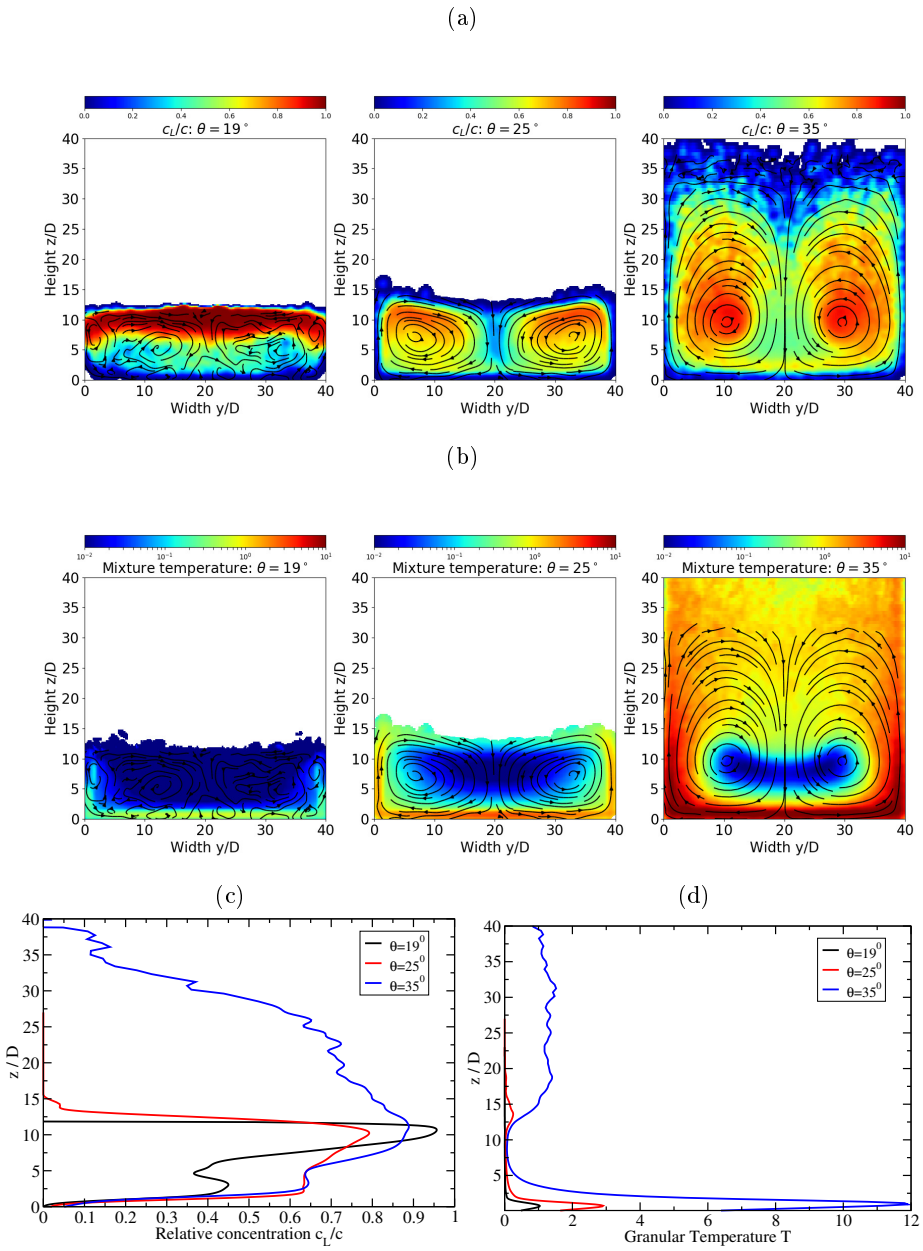

FIGURE 3. (a) Top panel : Bi-disperse flows ($2r_L = 1.5D$ and $2r_S = 0.75D$): Relative concentration of large particles c_L/c in the flow cross-section versus inclination angles for a mass fraction of small particles $\Phi_S = 0.5$. Streamlines are plotted to highlight the presence of convection rolls (black lines). (b) bottom panel: Corresponding maps of the granular temperature T of the mixture. (c) and (d): Vertical profiles of the relative volume fraction of the large particle, c_L/c, and of the granular temperature, computed at $y = 10D$.

segregation pattern is seen for an angle of 25°, for which the flow is not yet in a supported regime.

Fig. 4 shows the vertical position of the center of mass of the mixture together with that of the large and small particles, respectively, versus the tangent of the inclination

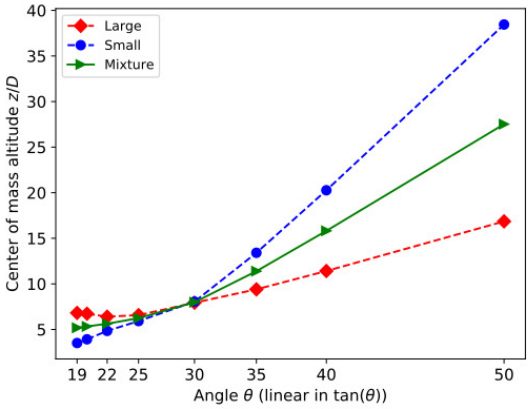

FIGURE 4. Vertical position of the center of mass of the mixture (solid line green triangle), large particles (dashed line red diamond) and small particles (dashed line blue dots) versus the inclination angle θ. $50-50$ mixture by mass with $2r_L = 1.5D$ and $2r_S = 0.75D$.

angle θ. Interestingly, an inversion in the vertical position of the center of mass of the large and small particles clearly appears between 25° and 30°, which corresponds to the range of angles in which supported flows develop for the set of parameters investigated. This unusual segregation pattern appears to be a direct consequence of the establishment of the supported flow. Furthermore, the linear relation between the center of mass and the tangent of the angle of inclination, derived by (Brodu *et al.* 2015) for supported flows ($\theta > 27°$) is also seen for a binary mixture and is robust to change of mixture composition.

4. Influence of the mixture concentration

The influence of the relative concentration of small particles Φ_S within the mixture was explored. We kept the same radii ratio of 2 as for previous simulations (i.e., $2r_L = 1.5D$ and $2r_S = 0.75D$). Profiles of streamwise velocity V_x are presented in Fig. 5.a for a low inclination angle, where dense flows are expected. The two limit cases (i.e., $\Phi_s = 0$ and 1) correspond to monodisperse flows with particles of diameter $2r_L = 1.5D$ and $2r_S = 0.75D$, respectively. The vertical velocity profiles corresponding these monodisperse flows indicate that the flow is uniformly sheared, with an ordering of grains in horizontal layers (Jenkins & Larcher 2017). The monosize flow with small particles is faster than the one with large particles, as predicted by Jenkins & Larcher (2017) for unconfined layered shear flows. In addition, decreasing the particle size while maintaining the width of the channel constant leads to a decrease of the lateral confinement exerted by the walls, resulting in an increase of the mean flow velocity. Theses two limit cases provide bounds for the comparison with binary mixtures.

Dense flow regimes of binary mixtures exhibit contrasting features. At any finite concentration investigated so far, the velocity profile looks like a plug flow with almost no shearing but a finite slip at the bottom. This is a consequence of the influence of the lateral boundaries. Note also that a weak concentration of small particles in the mixture ($\Phi_S = 0.05$ and 0.1) leads to a drastic reduction of the flow velocity in comparison with monodisperse flows of large particles. Mixture seems thus to prevent the formation of ordered layers, which slow the flow.

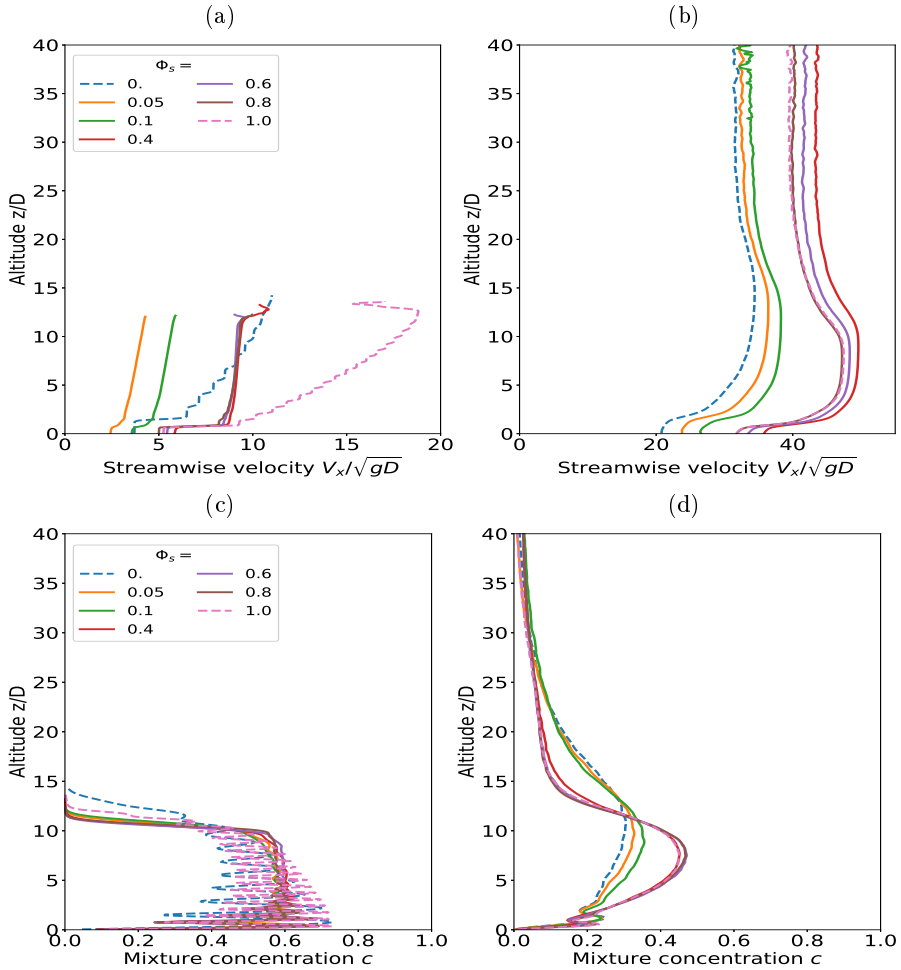

FIGURE 5. Vertical profiles of the streamwise velocity (a,b) and mixture concentration c (c,d) for binary mixtures with relative volume concentration of small particles Φ_S varying from 0 to 1: (a) and (c) dense regimes $\theta = 20°$, (b) and (d) supported regime $\theta = 35°$. Binary mixtures with $2r_L = 1.5D$ and $2r_S = 0.75D$.

A completely different behavior is observed for rapid flows, for which the supported regime is expected. Indeed, the slowdown for binary mixtures observed for dense flow regimes no longer exists and the streamwise velocity of mixtures are always higher than monodisperse flows of large particles (Fig. 5). Surprisingly, there is an optimal concentration of small particles (about $\Phi_S = 0.4$, see Fig. 5) that produces flows with velocities higher than the expected most favorable case, corresponding to a monodisperse flow of small particles. This is also seen in the flow of mixtures of a fluid and a binary mixtures of spheres above a particle bed (Larcher & Jenkins 2019).

The mass flow rate, which indicates the capacity of the flow to transport matter, is also highly influenced by the nature of the flow regime (dense versus supported). The variation of the mass flow rate as a function of the mixture concentration is reported in Fig. 6 for the dense and supported regimes, respectively. In the dense regime, the mass flow rate exhibits a plateau for mixture concentration Φ_S between 0.2 and 0.8. In this range of concentration, the mass flow rate is independent of the mixture concentration.

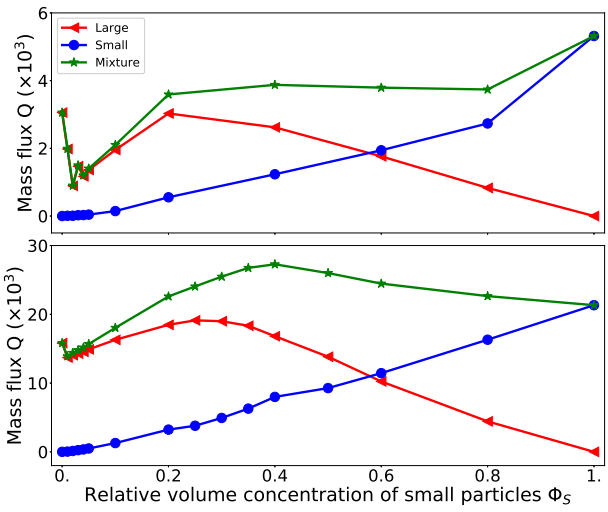

FIGURE 6. Mass flow rate Q (green stars) as a function of the relative volume concentration of small particles Φ_s in the mixture for dense flows at $\theta = 20°$ (top panel) and supported flows at $\theta = 35°$ (bottom panel). Q is the sum of the mass flow rate of the large (red triangles) and small (blue dots) particles.

This is simply a consequence of the invariance of the flow profiles in this concentration regime (cf. Fig 5). For small concentrations of the mixture, there is, in contrast, a drop of the mass flow rate which is mainly due to a decrease of the mass flow rate of the large particles. This drop is closely related to the decrease observed in the flow velocity profile for small mixture concentrations. The large concentration limit is also singular with an enhancement of the mass flow rate in comparison with the value of the plateau.

For the supported regime ($\theta = 35°$), an optimum of the mass flow rate emerges for a finite value of the mixture concentration: $\Phi_S \approx 0.4$. Moreover, a wide range of concentration provides a mass flow rate which is higher than the monodisperse case of small particles. The optimum seems to be governed by the large particles. Indeed, the mass flow rate of the large particles also displays an optimum for a finite concentration of the mixture (of order of $\Phi_S \approx 0.3$). In contrast, the mass flow rate of the small particles exhibits a monotone, regular increase with increasing mixture concentration. This result indicates that the establishment of the supported regime for a binary mixture promotes the transport capacity of the flow. The increase in transport efficiency is the result of the segregation process concentrating the large particles within the dense core, which is the most rapid part of the flow.

5. Interpretation and discussion

In dense gravity-driven flows, the larger particles often tend to rise at the top of the granular packing against gravity, usually associated with the kinetic sieving mechanism introduced by Savage & Lun (1988). At low inclination, we observe dense flows which exhibit such segregation. In contrast, at higher inclination, the observed segregation pattern is different. The large particle stand neither at the bottom of the flow nor at the top but are localized within the flow at rather constant elevation (i.e., at $z = 10D$). The large particle layer constitutes the densest part of the flow and is sandwiched between two dilute layers of fines (see Fig. 3.c). The elevation of the large particle layer corresponds to the location where the granular temperature is minimum (see Fig. 3.d).

The temperature difference between the dilute layer above the dense core and the dense core increases with increasing angle. This seems to indicate that the segregation is driven by temperature gradients. This is apparently different from segregation in gravity-driven flows at moderate inclination angle, but vertical temperature gradients can also play a role in these. Segregation driven by temperature gradients may be understood in the framework of the kinetic theory for binary mixtures of dense granular gases (Arnarson & Jenkins 2004; Garzó 2008, 2009; Larcher & Jenkins 2013, 2015; Jenkins & Larcher 2020). We anticipate that this kinetic theory, based on instantaneous, pairwise collisions alone, is, for the value of the sliding friction employed in the simulations, relevant until a mixture concentration of 0.60. For higher volume fractions, more enduring interactions at compliant contacts, associated with ephemeral force chains, become increasingly important (Berzi *et al.* 2020). This critical value of the concentration is a known function of the sliding friction, when the tangential coefficient is unity (Berzi & Vescovi 2015); we employ a slightly larger value for the lower value of tangential restitution in the simulations. We next employ this framework and outline the derivation of the equation that predicts a local measure of segregation in a binary mixture of spheres that do not differ much in size or mass. We then obtain two-dimensional solutions of this equation and compare the prediction with the data of the numerical simulations of a supported flow.

The balance of linear momentum for each type of sphere, written in terms of dimensional variables, has the form (e.g, Jenkins & Mancini (1987))

$$\frac{\partial}{\partial t}(\rho_I \mathbf{v}_I) + \nabla \cdot (\rho_I \mathbf{v}_I \mathbf{v}_I) = -\nabla \cdot \boldsymbol{\Pi}_I - n_I \mathbf{F}_I + \boldsymbol{\phi}_I \,, \tag{5.1}$$

where $I = L, S$ labels the two sizes of spheres, $\mathbf{v}_I$ is the species velocity, p_I the species pressure tensor, which in a dense flow contains only collisional contributions, $\mathbf{F}_I$ is the external force on a sphere I, and $\boldsymbol{\phi}_L = -\boldsymbol{\phi}_S$ are the forces of interaction between the two sizes of spheres. Segregation of the two sizes is predicted from the weighted difference of the momentum balances, when the inertia of the spheres is neglected and only the contributions of the partial pressures, p_L and p_S, to the pressure tensors are retained:

$$0 = -\frac{1}{\rho_L}\nabla p_L + \frac{1}{\rho_S}\nabla p_S - \frac{1}{m_L}\mathbf{F}_L - \frac{1}{m_S}\mathbf{F}_S + \frac{1}{\rho_L}\boldsymbol{\phi}_L - \frac{1}{\rho_S}\boldsymbol{\phi}_S \,, \tag{5.2}$$

in which the partial pressures are given in a dense flow by

$$p_L = (K_{LL} + K_{LS})T \text{ and } p_S = (K_{SS} + K_{SL})T \,, \tag{5.3}$$

where $K_{IJ} = (2/3)\pi n_I n_J r_{IJ}^3 g_{IJ}$, with $i = L, S$ and $J = L, S$; the radial distribution functions g_{IJ} for the two types of spheres will be given later in their approximate forms. This approximate form of the weighted difference of the balances of momentum of the two sizes of spheres provides an equation for predicting local segregation in the dense, inclined flow.

The Chapman-Enskog procedure for the determination of the velocity distribution function and constitutive relations for a dense binary mixture, as in Jenkins & Mancini (1989); Arnarson & Jenkins (2004); Larcher & Jenkins (2013, 2015), leads an expression for the difference in velocities of the two types of spheres:

$$\frac{n_L n_S}{n^2}\frac{1}{D_{LS}}(\mathbf{v}_L - \mathbf{v}_S) = \mathbf{d}_L + \frac{1}{T}K_T \nabla T \,, \tag{5.4}$$

where n_L and n_S are the two number densities, $n = n_L + n_S$; D_{LS} is the diffusion

coefficient,

$$D_{LS} = \frac{3}{2}\frac{1}{ng_{LS}}\left(\frac{2m_{LS}T}{\pi m_L m_S}\right)^{1/2}\frac{1}{8r_{LS}^2}\,; \tag{5.5}$$

and $\mathbf{d}_L$ is the diffusion force of the large spheres,

$$\mathbf{d}_L = -\frac{\rho_L}{\rho}\frac{1}{nT}\nabla P + \frac{1}{nT}\left(K_{LL} + 2\frac{m_L}{m_{LS}}K_{LS}\right)\nabla T + \frac{n_A}{nT}\left(\frac{\partial \mu_L}{\partial n_L}\nabla n_L + \frac{\partial \mu_L}{\partial n_S}\nabla n_S\right), \tag{5.6}$$

in which $P = p_L + p_S$ is the total pressure and μ_L is the chemical potential of the large spheres; and K_T is their thermal diffusion coefficient, all of which will also be given later in approximation. The expression for the velocity difference (5.4) has the same form of the weighted difference of the momentum balances (5.2), when the particle interaction $\boldsymbol{\phi}_S$ is taken to be

$$\begin{aligned}\boldsymbol{\phi}_S = &-K_{LS}\frac{m_S - m_L}{m_{LS}}\nabla T + \frac{n_L n_S}{n}T\frac{1}{D_{LS}}(\mathbf{v}_L - \mathbf{v}_S)\\ &+ n_L\frac{\partial}{\partial n_L}\left(\mu_L - \frac{p_L}{T}\right)\nabla n_L + n_L\frac{\partial}{\partial n_S}\left(\mu_L - \frac{p_L}{T}\right)\nabla n_S + nTK_T\nabla T\,.\end{aligned} \tag{5.7}$$

With the connection between (5.4) and (5.2) established, we adopt the (5.5) and (5.6) for the velocity differences and follow Arnarson & Jenkins (2004) and Larcher & Jenkins (2013, 2015) in employing approximations to g_{LS}, μ_L, and K_T that are linear in the small values of $\delta r = r_L/r_S - 1$ and $\delta m = (m_L - m_S)/m$, where, again, $m = m_S + m_L$. In addition, we here retain only those terms that dominate in the dense limit, and express these in terms of the measure of segregation $X = (n_L - n_S)/(2n)$. The segregation index X is the local difference in number fractions of the two sizes of spheres; at points at which it is 0, there is no segregation; where it is $1/2$, there are only large spheres; and where it is $-1/2$ there are only small spheres. Because X varies between $-1/2$ and $1/2$, we also ignore products of it with δr and δm. Then, when expressed in terms of the mixture concentration, c, and $\lambda = c(3-c)/(2-c)$ the approximation to the radial distribution functions for a binary mixture given by (e.g., Larcher & Jenkins (2015))

$$g_{LL} \approx \tfrac{G}{c}(1 + 0.5\lambda\delta r) \qquad \text{and } K_{LL} \approx 4\frac{n_L^2}{n}G\left[1 + 0.5\,(3+\lambda)\,\delta r\right] \tag{5.8}$$

$$g_{SS} \approx \tfrac{2-\nu}{2(1-\nu)^3}(1 - 0.5\lambda\delta r) \;\text{ and } K_{SS} \approx 4\frac{n_S^2}{n}G\left[1 - 0.5\,(3+\lambda)\,\delta r\right] \tag{5.9}$$

and

$$g_{LS} \approx \frac{G}{c} \text{ and } K_{LS} \approx 4G\frac{n_L n_S}{n} \tag{5.10}$$

in which, we regard the mixture as a single phase of identical spheres of radius $r \equiv (r_S + r_L)/2$ and concentration $c \approx (4\pi/3)r^3 n(1 + 3X\delta r)$, and take $G/c \equiv 5.69(c_M - 0.49)/(c_M - c)$, the dense contact radial distribution function of Torquato (1995), with a singularity at the critical volume fraction c_M, rather than that Mansoori *et al.* (1971), appropriate for lower volume fractions, with a singularity at unity,

$$\frac{\partial \mu_L}{\partial n_L} \approx \frac{4}{n}\left(1 + 6\frac{n_S}{n}\delta r\right)cHT \text{ and } \frac{\partial \mu_L}{\partial n_S} \approx \frac{4}{n}\left(1 - 6X\delta r\right)cHT\,, \tag{5.11}$$

where $H \equiv dG/dc = G(c_M/c)/(c_M - c)$; and

$$K_T \approx \frac{n_L n_S}{29n^2}\left(-6\delta r + 63\delta m\right)\,. \tag{5.12}$$

With these, when the only external force is the vector of the gravitational acceleration,

g, the contributions from the external forces cancel, and (5.4) and (5.6) yield

$$\frac{n_L n_S}{n^2}\frac{1}{D_{LS}}(\mathbf{v}_L-\mathbf{v}_S)=-\frac{\rho_L}{\rho}\frac{1}{nT}\nabla P+\frac{n_L}{n}4G\left[1+\frac{1}{2}\frac{n_S}{n}(3+\lambda)\delta r+\frac{n_S}{n}\delta m\right]\frac{\nabla T}{T}$$
$$+\frac{3}{29}\frac{n_L n_S}{n^2}G\left(-2\delta r+21\delta m\right)\frac{\nabla T}{T}+\frac{n_L}{n^2}\left[\left(\frac{n}{n_L}+4cH+24cH\frac{n_S}{n}\delta r\right)\nabla n_L+4cH\nabla n_S\right]. \tag{5.13}$$

The spatial gradients of $n_L = n(0.5+X)$ and $n_S = n(0.5-X)$ may be expressed in terms of those of c and X using the approximations

$$\nabla n_L \approx \frac{3c}{4\pi r^3}(0.5+X)\frac{\nabla c}{c}+\frac{3c}{4\pi r^3}(1-1.5\delta r)\nabla X \tag{5.14}$$

and

$$\nabla n_S \approx \frac{3c}{4\pi r^3}(0.5-X)\frac{\nabla c}{c}-\frac{3c}{4\pi r^3}(1+1.5\delta r)\nabla X. \tag{5.15}$$

Then

$$\frac{n_S}{n}\frac{1}{D_{LS}}(\mathbf{v}_L-\mathbf{v}_S)=-\frac{m_L}{\rho}\frac{1}{T}\nabla P+4G\left[1+\frac{1}{2}\frac{n_S}{n}(3+\lambda)\delta r+\frac{n_S}{n}\delta m\right]\frac{\nabla T}{T}$$
$$+\frac{3}{29}\frac{n_S}{n}G\left(-2\delta+21\delta m\right)\frac{\nabla T}{T}+\frac{n}{n_L}\nabla X+4cH(1+1.5\delta r)\frac{\nabla c}{c}. \tag{5.16}$$

The mixture pressure P is given in terms of the mixture concentration, in approximation, as

$$P\approx 4nGT=4\frac{3c}{4\pi r^3}GT=\frac{3c}{\pi r^3}GT\,. \tag{5.17}$$

Then, when only gravity is present, the sum of the species momentum balances of (5.1) is

$$\nabla P=\rho\mathbf{g}\,; \tag{5.18}$$

or, upon using (5.17) and $\rho\approx 3/(4\pi r^3)(m/2)c$,

$$4cH\frac{\nabla c}{c}-12G\delta r\nabla X+4G\frac{\nabla T}{T}=\frac{m}{2}\frac{\mathbf{g}}{T}\,. \tag{5.19}$$

With this, the concentration gradient may be eliminated from (5.16):

$$\frac{\mathbf{v}_L-\mathbf{v}_S}{D_{LS}}=4G\left[\left(\frac{1}{2}(3+\lambda)-\frac{177}{58}\right)\delta r+\frac{179}{116}\delta m\right]\frac{\nabla T}{T}+\frac{m}{2}(3\delta r-2\delta m)\frac{\mathbf{g}}{T}+\frac{n^2}{n_L n_S}\nabla X\,. \tag{5.20}$$

We apply this equation to a steady, fully-developed flow in which the diffusion velocities vanish.

We make the approximations that the mixture concentration in the dense part of the flow is uniform and equal to 0.59. Then, $\lambda = 1.01$, $G = 6.49$, and, with $\mathbf{g}{=}{-}g\cos\theta\mathbf{k}$, where the unit vector $\mathbf{k}$ is normal to the flow and directed upward, Eq. (5.20) has the dimensionless form

$$\nabla\left[\ln\left(\frac{1+2X}{1-2X}\right)^{1/2}+(6.2\delta m-4.2\delta r)\,G\ln w\right]=-\left(\delta m-1.5\delta r\right)\frac{\cos\theta}{w^2}\,\mathbf{k}, \tag{5.21}$$

where $w^2 \equiv 2T/(mgD)$. The assumption made regarding the uniformity of the mixture concentration, and its value, are in rough agreement with the measurements in the neighborhood of the segregation features in the simulations.

(a) (b)

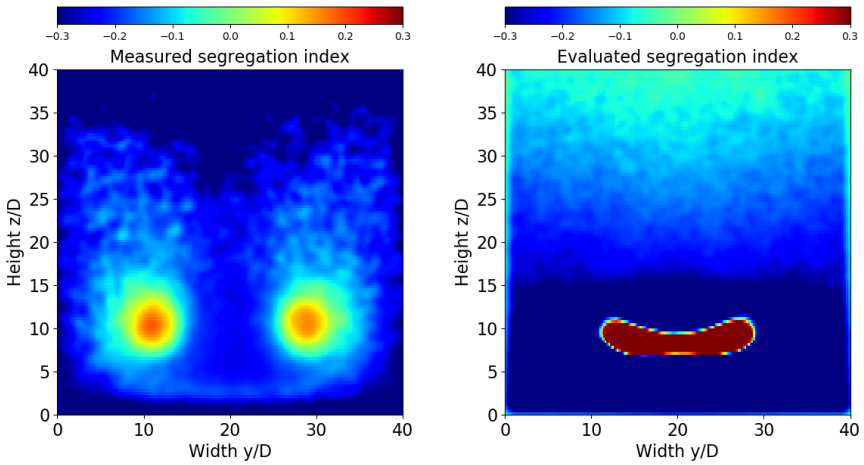

FIGURE 7. (a) The values of the segregation index X measured in the numerical simulation for a 50/50 mixture in mass with $r_L/r_S = 1.35$ (i.e., $\delta r = 0.35$); and (b) the values of X predicted by the theory.

If the spheres are made of the same material, $\delta m = 1.5\delta r$. In this case, the right-hand side of Eq. (5.21) vanishes and, with our assumption of the uniformity of the concentration, gravity influences segregation only through the temperature. Then, $6.2\delta m - 4.2\delta r = 5.1\delta r$, and Eq. (5.21) may be written as

$$\nabla \left[\ln \left(\frac{1+2X}{1-2X} \right)^{1/2} + 5.1 G \delta r \ln w \right] = 0. \tag{5.22}$$

The integral of this equation is

$$X = \frac{1}{2} \frac{w_0^{10.2G\delta r} - w^{10.2G\delta r}}{w_0^{10.2G\delta r} + w^{10.2G\delta r}}, \tag{5.23}$$

where w_0 is the value of w at which $X = 0$.

In Figure 7 we compare values of the segregation index X, based on the fields of temperature and concentration measured in the simulations, with those predicted by Eq. (5.23) for a 50/50 mixture in mass with $r_L/r_S = 1.35$ (i.e., $\delta r = 0.35$). The location of the segregation is roughly the same, but the centers of the segregation patterns in the simulations are distinct and separated. In our view, the difference in the patterns is due to the presence of convection, which is not incorporated in the theory. The convection rolls result in mixing that brings smaller spheres into the center of the flow and creates what appears to be a more intense segregation between them. Consequently, the predicted pattern of segregation shows less contrast between the rolls and their centers are not so distinct and clearly separated.

6. Conclusion

We have outlined the features of a regime of rapid inclined flow of a binary mixture of spheres as seen in discrete numerical simulations. The regime occurs at relatively high inclinations and involves enhanced transport that is associated with the development

of circulation secondary flows and the concentration of the larger spheres within them in response to gradients of granular temperature. This is in contrast to denser flows at lower inclinations that exhibit a simpler segregation pattern with larger spheres at the top, often associated with percolation of the smaller spheres, but also explained as due to gradients of granular temperature. We have also characterized the ratio of mass fraction of small spheres that provides the greatest enhancement of the rapid flows. Finally, we have indicated that the observed segregation patterns in the rapid flows are consistent with the predictions of a kinetic theory for binary mixtures that incorporates the influence of gradients of granular temperature on the segregation.

Additional discrete numerical simulations are necessary to further understand the details of the parameter space, particularly the influence of the particle properties on the flow and segregation in the rapid flows. Also, it would be useful to develop numerical solutions to the continuum equations of the kinetic theory to predict the two-dimensional fields of mixture concentration, velocity, and granular temperature in dense, steady, fully-developed inclined flows. This would permit a complete comparison between the predictions of the theory and what is seen in the discrete numerical simulations.

Funding. A.N., R.D. and A.V. acknowledge the support of the French Research National Agency through the project ANR-16-CE01-0005.

Declaration of interests. The authors report no conflict of interest.

REFERENCES

Arnarson, B. Ö. & Jenkins, J. T. 2004 Binary mixtures of inelastic spheres: Simplified constitutive theory. *Phys. Fluids* **16** (12), 4543–4550.

Berzi, Diego, Jenkins, James T. & Richard, Patrick 2020 Extended kinetic theory for granular flow over and within an inclined erodible bed. *J. Fluid Mech.* **885**, A27.

Berzi, D. & Vescovi, D. 2015 Different singularities in the functions of extended kinetic theory at the origin of the yield stress in granular flows. *Phys. Fluids* **27** (1), 013302.

Brodu, N., Delannay, R., Valance, A. & Richard, P. 2015 New patterns in high-speed granular flows. *J. of Fluid Mech.* **769**, 218–228.

Brodu, N., Richard, P. & Delannay, R. 2013 Shallow granular flows down flat frictional channels: Steady flows and longitudinal vortices. *Phys. Rev. E* **87** (2), 11–13.

D'Ortona, U. & Thomas, N. 2020 Self-induced rayleigh-taylor instability in segregating dry granular flows. *Phys. Rev. Lett.* **124**, 178001.

Garzó, V. 2008 Brazil-nut effect versus reverse brazil-nut effect in a moderately dense granular fluid. *Phys. Rev. E* **78**, 020301.

Garzó, V. 2009 Segregation by thermal diffusion in moderately dense granular mixtures. *Eur. Phys. J. E* **29**, 261–274.

Gray, J. M. N. T. & Ancey, C. 2011 Multi-component particle-size segregation in shallow granular avalanches. *J. Fluid Mech.* **678**, 535–588.

Gray, J. M. N. T. & Thornton, A. .R 2005 A theory for particle size segregation in shallow granular free-surface flows. *Proc. R. Soc. A* **461**.

Hill, K. M., Gioia, G. & Amaravadi, D. 2004 Radial segregation patterns in rotating granular mixtures: Waviness selection. *Phys. Rev. Lett.* **93**, 224301.

Jenkins, J. T. & Larcher, M. 2017 Dense, layered, inclined flows of spheres. *Phys. Rev. Fluids* **2**, 124301.

Jenkins, J. T. & Larcher, M. 2020 Segregation in a dense, inclined, granular flow with basal layering. *Granul. Matter* **22**, 1434–1436.

Jenkins, J. T. & Mancini, F. 1987 Balance Laws and Constitutive Relations for Plane Flows

of a Dense, Binary Mixture of Smooth, Nearly Elastic, Circular Disks. *J. Appl. Mech.* **54** (1), 27–34.

Jenkins, J. T. & Mancini, F. 1989 Kinetic theory for binary mixtures of smooth, nearly elastic spheres. *Phys. Fluids A* **1** (12), 2050–2057.

Khakhar, D. V., McCarthy, J. J. & Ottino, J. M. 1997 Radial segregation of granular mixtures in rotating cylinders. *Phys. Fluids* **9** (12), 3600–3614.

Larcher, M. & Jenkins, J.T. 2019 The influence of granular segregation on gravity-driven particle-fluid flows. *Adv. Water Resour.* **129**, 365 – 372.

Larcher, M. & Jenkins, J. T. 2013 Segregation and mixture profiles in dense, inclined flows of two types of spheres. *Phys. Fluids* **25** (11), 113301.

Larcher, M. & Jenkins, J. T. 2015 The evolution of segregation in dense inclined flows of binary mixtures of spheres. *J. Fluid Mech.* **782**, 405–429.

Louge, M. Y. & Keast, S. C. 2001 On dense granular flows down flat frictional inclines. *Phys. Fluids* **13** (5), 1213–1233.

Mansoori, G. A., Carnahan, N. F., Starling, K. E. & Leland, T. W. 1971 Equilibrium thermodynamic properties of the mixture of hard spheres. *J. Chem. Phys.* **54** (4), 1523–1525.

Pouliquen, O., Delour, J. & Savage, S. B. 1997 Fingering in granular flows. *Nature* **386**, 816–817.

Richard, P., Valance, A., Métayer, J. F., Sanchez, P., Crassous, J., Louge, M. & Delannay, R. 2008 Rheology of confined granular flows: Scale invariance, glass transition, and friction weakening. *Phys. Rev. Lett.* **101** (24), 1–4.

Savage, S. B. & Lun, C. K.K. 1988 Particle size segregation in inclined chute flow of dry cohesionless granular solids. *J. Fluid Mech.* **189**, 311–335.

Serero, D., Goldenberg, C., Noskowicz, S. H. & Goldhirsch, I. 2008 The classical granular temperature and slightly beyond. *Powder Technol.* **182** (2), 257–271.

Taberlet, N., Richard, P., Jenkins, J. T. & Delannay, R. 2007 Density inversion in rapid granular flows: the supported regime. *Eur. Phys. J. E* **22** (1), 17–24.

Torquato, S. 1995 Nearest-neighbor statistics for packings of hard spheres and disks. *Phys. Rev. E* **51**, 3170–3182.

Weinhart, T., Thornton, A. R., Luding, S. & Bokhove, O. 2012 From discrete particles to continuum fields near a boundary. *Granul. Matter* **14** (2), 289–294.

Zhu, Y., Delannay, R. & Valance, R. 2021 Discrete numerical simulations of high-speed granular flows: Influence of the side-walls. *Preprint* .